Cryoclastic origin of particles on the surface of Enceladus

W. Degruyter[1] and M. Manga[1]

Received 10 June 2011; revised 14 July 2011; accepted 15 July 2011; published 19 August 2011.

[1] Analogous to volcanic deposits on Earth, we can infer eruption characteristics on Enceladus from the relationship between particle size and distance from the vent. We develop a model in which ice particles feeding plumes are accelerated by the gas. We consider two cases: drag-limited and collision-limited acceleration, which link particle size to exit velocity. After being ejected at the vent, particles follow ballistic trajectories. We fit the model to observations of particle size on the surface inferred from modeled VIMS data collected by the Cassini spacecraft. We obtain a relationship between gas temperature and characteristic acceleration length, whereby lower gas temperatures require longer acceleration lengths. The model shows that the large size of particles on the surface is consistent with the size of particles observed with the CDA and VIMS instruments at heights of Cassini flybys, and the size of particles that reach escape velocity and are found in Saturn's E-ring. **Citation:** Degruyter, W., and M. Manga (2011), Cryoclastic origin of particles on the surface of Enceladus, *Geophys. Res. Lett.*, *38*, L16201, doi:10.1029/2011GL048235.

1. Introduction

[2] The Cassini spacecraft discovered active cryovolcanism on the South Polar Terrain of Enceladus, a small icy moon of Saturn [*Porco et al.*, 2006]. A heat source was observed along four parallel cracks dubbed "tiger stripes" [*Spencer et al.*, 2006], where plumes originate at localized sources [*Hansen et al.*, 2008]. These plumes eject primarily water vapor [*Waite et al.*, 2006] with entrained ice grains feeding the E-ring of Saturn [*Spahn et al.*, 2006]. The relatively slow velocities of the ice particles compared to the gas velocity and the origin of the ice grains have been an active topic of debate [*Porco et al.*, 2006; *Kieffer et al.*, 2006; *Fortes*, 2007; *Schmidt et al.*, 2008; *Brilliantov et al.*, 2008; *Halevy and Stewart*, 2008]. Here we present an additional constraint to test potential hypotheses by interpreting the size of particles adjacent to the tiger stripes as being cryovolcanic in origin.

[3] The distribution of ice particles on Enceladus as derived from VIMS measurements shows an increase of ice particle size near the fractures [*Jaumann et al.*, 2008]. We assume this distribution is explained by deposition of ice particles that are ejected from the cracks and explore the implications of this assumption. Two mechanisms for accelerating the ice particles are investigated: drag-limited and collision-limited acceleration. We use a ballistic model to describe the trajectory of the ice particles once they exit the vent. The model predictions are then fitted to data from *Jaumann et al.* [2008] to constrain the characteristic acceleration length and the temperature of the gas. From these results we calculate the maximum height to which different size particles are ejected and discuss these sizes in light of measurements during Cassini flybys.

2. Model

[4] We assume that the plumes are sourced from cracks, and ice particles are accelerated by the gas within the cracks. Following *Ingersoll and Pankine* [2010], we assume all gas properties are determined by its temperature T. The gas pressure P is the saturation vapor pressure given by

$$P = a_1 \exp\left(\frac{-a_2}{T}\right), \tag{1}$$

where a_1 and a_2 are fitting constants. Assuming an ideal gas, the gas density ρ_g is then

$$\rho_g = \frac{P}{RT} = \frac{Pm_0}{k_B T} \tag{2}$$

where R is the specific gas constant of water, m_0 the mass of a water molecule, and k_B the Boltzmann constant. We assume that the gas flow is choked, thereby setting the gas velocity u_g equal to the sound speed for saturated gas

$$u_g = \sqrt{RT}. \tag{3}$$

The gas viscosity η is given by the empirical law

$$\eta = b_1 \left(\frac{T}{b_2}\right)^{b_3} \tag{4}$$

where b_1, b_2 and b_3 are fitting constants. Constants and variables are listed in Table 1.

2.1. Drag-Limited Acceleration

[5] The acceleration of a spherical particle in a gas is described by [e.g., *Crowe et al.*, 1997]

$$M_p \frac{du_p}{dt} = \frac{1}{2}\rho_g C_D \pi R_p^2 |u_g - u_p|(u_g - u_p) \tag{5}$$

where u_p, R_p, $M_p = \rho_p \frac{4\pi}{3} R_p^3$, and ρ_p are the ice particle velocity, radius, mass, and density respectively. The drag coefficient C_D is a function of the Reynolds number (Re) and the Mach number (Ma) [*Crowe et al.*, 1997]

$$\mathrm{Re} = \frac{\rho_g(u_g - u_p)2R_p}{\eta}, \quad \mathrm{Ma} = \frac{u_g - u_p}{\sqrt{RT}}. \tag{6}$$

The (Re, Ma)-map is subdivided into different flow regimes according to the Knudsen number (Kn), the ratio

[1]Earth and Planetary Science and Center for Integrative Planetary Science, University of California, Berkeley, California, USA.

0094-8276/11/2011GL048235

Table 1. Constants and Variables Used in the Model

	Symbol	Value	Unit
fitting constants equation (1)	a_1	3.63×10^{12}	Pa
	a_2	6147	K
fitting constants equation (4)	b_1	0.925×10^{-5}	Pa s
	b_2	300	K
	b_3	1.1	
Boltzmann constant	k_B	1.38065×10^{-23}	J K^{-1}
mass of a water molecule	m_0	2.992×10^{-26}	kg
specific gas constant of water	$R = \frac{k_B}{m_0}$	461.4	J kg^{-1} K^{-1}
density of ice particle	ρ_p	920	kg m^{-3}
gravitational acceleration	g	0.11	m s^{-2}
radius Enceladus	R_E	252×10^3	m
ejection angle	γ_0	65	°
particle radius	R_p	10^{-7}–10^{-3}	m
characteristic acceleration length	L_d, L_c	0.1–100	m
gas temperature	T	190–273	K

of the mean-free path of gas molecules to the particle size

$$\mathrm{Kn} = \frac{\eta}{\rho_g 2R_p}\sqrt{\frac{\pi m_0}{2k_B T}} = \sqrt{\frac{\pi}{2}}\frac{\mathrm{Ma}}{\mathrm{Re}}. \quad (7)$$

For particle sizes between 100 nm and 1 mm and temperatures between 190 K and 273 K, Kn is between 10^{-3} and 10^5. This covers a large range of flow regimes from free molecular (Kn > 10), to transitional (0.25 < Kn < 10) and slip flow (10^{-3} < Kn < 0.25), and to a continuum (Kn < 10^{-3}) [*Crowe et al.*, 1997]. *Crowe et al.* [1997] suggest the following empirical formula for C_D to cover this broad range of Kn

$$C_D = 2 + \left(\frac{24 f_1}{\mathrm{Re}} - 2\right)\exp\left(-3.07 f_2 \frac{\mathrm{Ma}}{\mathrm{Re}}\right) + \frac{f_3}{\mathrm{Ma}}\exp\left(-2\frac{\mathrm{Re}}{\mathrm{Ma}}\right) \quad (8)$$

$$f_1 = 1 + 0.15\,\mathrm{Re}^{0.687} + \frac{0.0175}{1 + 42500\,\mathrm{Re}^{-1.16}} \quad (9)$$

$$f_2 = \frac{1 + \mathrm{Re}(12.278 + 0.548\,\mathrm{Re})}{1 + 11.278\,\mathrm{Re}} \quad (10)$$

$$f_3 = \frac{5.6}{1 + \mathrm{Ma}} + 1.7 \quad (11)$$

We note that this model predicts qualitatively similar results to *Schmidt et al.* [2008] when Kn $\gg$ 1. For Re $\ll$ 1 and Ma $\ll$ 1, the drag coefficient converges to simple Stokes drag C_D = 24/Re. This acceleration model is deterministic, i.e., the velocity a particle can reach is determined by its size R_p, the length L_d over which it is allowed to accelerate, and the gas temperature T (Figure 1).

2.2. Collision-Limited Acceleration

[6] The acceleration of particles can also be limited by the distance they are allowed to travel between collisions owing to being confined between the crack walls [*Schmidt et al.*, 2008]. We follow the assumptions of *Schmidt et al.* [2008] that wall collisions are described by a random Poisson process. This acceleration model is stochastic, i.e., the velocity a particle can reach is not uniquely determined, but can be described by an average with a standard deviation for a given size R_p, the characteristic length L_c between collisions, and the gas temperature T. The contribution of previous collisions scales as e^N, with e the restitution coefficient ($0 \le e \le 1$) and N the number of collisions [*Brilliantov et al.*, 2008]. When e = 1, the results are the stochastic equivalent of the drag-limited case ($L_c = L_d$). Therefore, like *Schmidt et al.* [2008], we only consider the case where particle velocities are reset to zero after a collision (e = 0), and note that drag-limited and collision-limited acceleration are end-member cases of the same model. Using Monte Carlo simulations to imitate a random Poisson process in combination with equation (5) we obtain an average particle velocity for a given characteristic collision length L_c and gas temperature T (Figure 1). For comparison, ISS observations suggest an average particle velocity of 60 m s^{-1} [*Spencer et al.*, 2009] and VIMS observations estimate a range between 80 and 180 m s^{-1} [*Hedman et al.*, 2009].

2.3. Ballistic Model

[7] To describe the trajectory of a particle once it is ejected from the crack, we assume the particle is moving in a vacuum and is not further accelerated by the gas. When the gas decompresses the density drops several orders of magnitude, dramatically decreasing the drag coefficient C_D. The resulting acceleration from the gas will therefore be negligible. Consider the initial conditions for the particle position (x_0 = 0, $y_0 = R_E$) or in polar coordinates ($r_0 = R_E$, $\theta_0 = \frac{\pi}{2}$) and exit velocity ($v_{x0} = u_p$

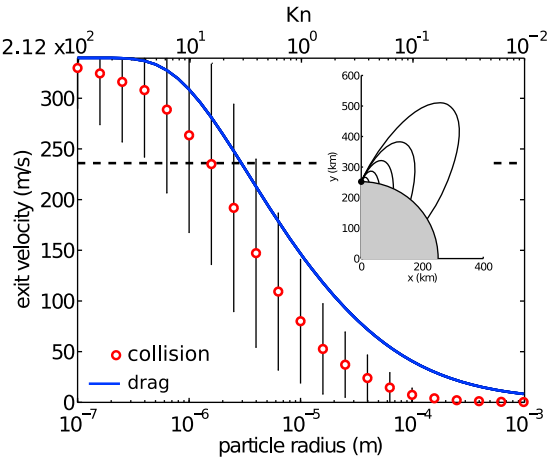

Figure 1. Particle radius versus exit velocity for $L_d = L_c$ = 0.1 m and T = 250 K ($u_g = \sqrt{RT}$ = 340 m s^{-1}). The Knudsen number for T = 250 K is shown on the top axis. The full blue line is calculated from equation (5). The red points are calculated from averaging the velocity obtained from Monte Carlo simulations of a Poisson process with equation (5). The error bars indicate 1 standard deviation. The black dashed curve represents the escape velocity of 235 m s^{-1}. Inset: Particle trajectories (black) calculated for exit velocities between v_0 = 60 m s^{-1} and v_0 = 180 m s^{-1} with increments of 30 m s^{-1}. Enceladus is represented by the gray circle.

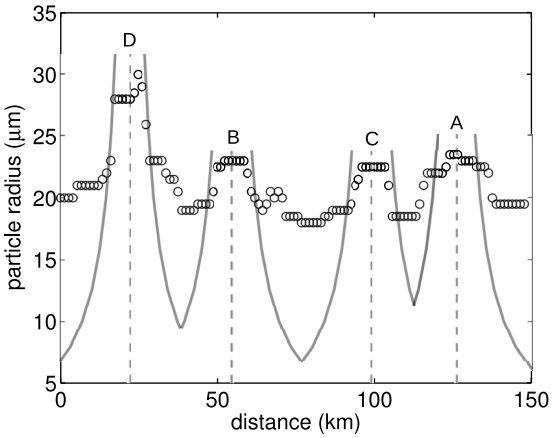

Figure 2. The open black circles indicate particle sizes derived from VIMS measurements at a cross section taken perpendicular to the tiger stripes [*Jaumann et al.*, 2008]. The dashed black lines indicate assumed crack positions of 22 km at Damascus (D), 55.5 km at Baghdad (B), 99 km at Cairo (C), and 126 km at Alexandria. The gray curves are calculated by applying drag-limited acceleration, assuming L_d = 1.7 m, T = 220 K ($u_g = \sqrt{RT}$ = 319 m s^{-1}) and using the ballistic equations.

cos γ_0, $v_{y0} = u_p$ sin γ_0), where γ_0 is the ejection angle. The governing ballistic equations are

$$\frac{dv_x}{dt} = -g\left(\frac{R_E}{r}\right)^2 \cos\theta, \tag{12}$$

$$\frac{dv_y}{dt} = -g\left(\frac{R_E}{r}\right)^2 \sin\theta \tag{13}$$

We treat γ_0 as a constant throughout this study and set it equal to 65°, the angle the plume edge is believed to make with the surface [*Schmidt et al.*, 2008]. Examples of possible trajectories are shown in the inset of Figure 1.

3. Results

[8] The model is used to fit the particle sizes provided by *Jaumann et al.* [2008] (Figure 2). A reasonable agreement between the model and the derived observations can be found at intermediate distances (5–10 km) from the cracks. At shorter distances a maximum in particle size is observed and further away from the crack the particle sizes are larger than model predictions. We fit our model to the measurements of the Damascus peak (with crack position at 22 km) to find a correlation between gas temperature and characteristic acceleration length by calculating the χ^2 value over a range of gas temperatures and acceleration lengths (Figure 3). For drag-limited acceleration we obtain:

$$\log_{10} L_d = -0.055455T + 12.435, \tag{14}$$

and for collision-limited acceleration:

$$\log_{10} L_c = -0.042783T + 10.633, \tag{15}$$

where L is in m and T is in K. To fit the deposit a particle of a certain size will have to be accelerated less if the length over which it can be accelerated is longer. This requires a smaller value for the drag coefficient C_D, which is achieved by a decrease in gas temperature, as this decreases the pressure (equation (1)), density (equation (2)), and gas velocity (equation (3)). We note that small variations in both temperature and acceleration length lead to large differences in predicted deposition as is evident from Figure 3.

4. Discussion

[9] The model predicts smaller particle sizes than the sizes observed at large distances (>10 km) from the crack. This discrepancy also appears in other models of particle deposition that predict small particle sizes at these distances [*Kempf et al.*, 2010]. Assuming the data interpretation by *Jaumann et al.* [2008] that the ice particles are made off pure water ice is correct we discuss several mechanisms for discrepancies. In order for grain growth processes to be effective their timescale has to be faster than the particle deposition time scale which is 0.5 mm/year in the vicinity of the jets and drops of to 10^{-5} mm/year near the equator [*Kempf et al.*, 2010]. Grains can grow by sintering [*Kaempfer and Schneebeli*, 2007] or sputtering [*Clark et al.*, 1983], but the timescales are likely to be very large at surface temperature of ~80 K [*Spencer et al.*, 2006]. We therefore expect that altering the deposits by grain growth is slower than regenerating them by deposition near the plumes, but might become relevant further away from the cracks. Another possibility is changing of the crack geometry over time, whereby the crack in the early stages of its existence was wider and could deposit particles further as the characteristic acceleration length would be longer. An increase of the acceleration length by a factor of 2 could explain particles with radii of 20 μm at >20 km distance. The maximum size of particles at distances close to the crack (<5 km) may be limited by the mechanism that produces the particles, but larger particle sizes do exist close to the center of the tiger stripes. *Jaumann et al.* [2008] report 0.2 mm particles at the tiger stripes and the VIMS instrument loses sensitivity for particles not much larger than this. ISS images blocks 10s of m in size [*Porco et al.*, 2006].

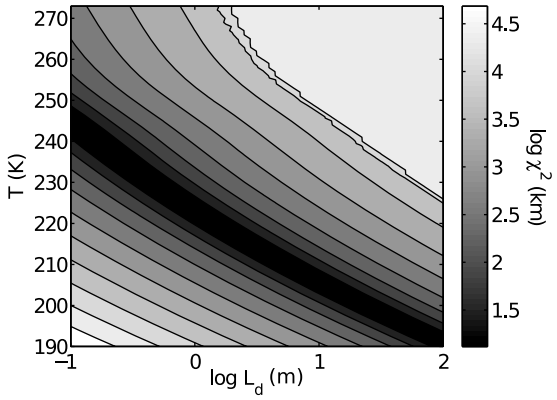

Figure 3. Map of log(χ^2) value obtained by fitting predictions of drag-limited acceleration to slope data points of the crack at Damascus in Figure 2. The best fit (black region) follows a trend where a higher temperature requires a shallower starting depth. Fitting of minimum χ^2 value relates the temperature T with the starting depth L_d (equation (14)).

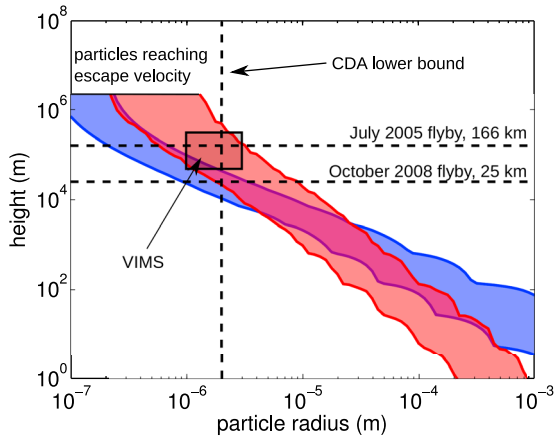

Figure 4. Maximum particle height versus particle radius. The shaded areas show the solution for a gas temperature range T = 190–273 K using the best fit for the acceleration length. The blue area is obtained by applying drag-limited acceleration and the red area by applying collision-limited acceleration. These predictions are in agreement with several observations including particle sizes measured by VIMS [*Hedman et al.*, 2009], particles collected by the CDA [*Spahn et al.*, 2006], and the particle sizes that reach the escape velocity and feed the E-ring [*Kempf et al.*, 2010]. The wiggles in the curves for larger particle sizes are attributed to intermediate Kn, where particles experience several flow regimes during acceleration.

[10] An independent way of testing our interpretation is by predicting the height reached for a given particle radius (Figure 4). The drag-limited model predicts lower heights than the collision-limited model for small (<10 μm) particle sizes. The collision-limited model agrees best with constraints on the size of erupted particles: (i) the Cosmic Dust Analyzer sampled particles >2 μm at an altitude of 166 km during the July 2005 flyby [*Spahn et al.*, 2006], (ii) *Hedman et al.* [2009] obtained VIMS measurements during the November 2007 flyby that showed the dominant particle size between 49 km and 279 km is between 1 and 3 μm, (iii) the particle sizes feeding Saturn's E-ring are <1 μm [*Kempf et al.*, 2010], and (iv) the Cassini spacecraft could be destroyed if it collides with a particle larger than 1 mm [*Razzaghi et al.*, 2007]. Our model predicts such an encounter is unlikely as the closest flyby is at 25 km altitude and 1 mm particles will only be propelled a couple of meters to 100 m high.

[11] Several suggestions have been made in the literature for the origins of the ice particles: (i) the particles are created by a phase change after explosive boiling of subsurface liquid water by sudden decompression created by opening of a crack (Cold Faithful model [*Porco et al.*, 2006]) or by particle nucleation and growth during ascent of the gas within the cracks [*Schmidt et al.*, 2008], (ii) the particles have a mechanical origin by fragmentation of clathrates (Frigid Faithful model [*Kieffer et al.*, 2006]), or by tidal stresses acting on crack walls [*Nimmo et al.*, 2007; *Hurford et al.*, 2007], which produce materials similar to fault gouge by shearing and brecciation. These particles would then be entrained by escaping gas. The drag-limited particle acceleration can only describe particles that form at shallow depths, within the upper few meters of the surface. For collision-limited acceleration there is no need for this assumption as particles only carry information from their last collision. Although no generation mechanism can be excluded, a large range of sizes (10^{-7} to $>10^{-4}$ m) exists and must be accounted for.

[12] Owing to the trade-off between temperature and acceleration length, our model for the ejection and deposition of ice particles does not exclude any of the proposed models for the origin of particles. However, it provides constraints as knowledge of the gas temperature determines the acceleration length and vice versa. For example, *Kieffer et al.* [2006] suggest a temperature of 190 K for a shallow clathrate reservoir which would imply an acceleration length around 100 m. Alternatively, an upper bound for the crack width can be estimated as 5 m, the diurnal tidal amplitude [*Hurford et al.*, 2007]. If we assume the acceleration length ~ crack width, the required temperature is >215 K in agreement with estimates of *Abramov and Spencer* [2009].

[13] In conclusion, if the size distribution of particles adjacent to the tiger stripes reflects their deposition from a vent, we obtain new insights into the eruptions. More accurate determination of particle size distributions around the tiger stripes can lead to a more detailed description of the crack geometry and vent temperature, as well as the variation of these quantities along the fractures.

[14] **Acknowledgments.** We thank Edwin Kite for useful suggestions and discussions and Ralf Jaumann for generously providing the particle size data. Sue Kieffer and an anonymous reviewer greatly improved this paper. WD was supported by a Fellowship of the Belgian American Educational Foundation. Additional funding was provided by the NASA PGG program.

[15] The Editor thanks Susan Kieffer and an anonymous reviewer for their assistance in evaluating this paper.

References

Abramov, O., and J. R. Spencer (2009), Endogenic heat from Enceladus' south polar fractures: New observations, and models of conductive surface heating, *Icarus*, *199*, 189–196.

Brilliantov, N., J. Schmidt, and F. Spahn (2008), Geysers of Enceladus: Quantitative analysis of qualitative models, *Planet Space Sci*, *56*, 1596–1606.

Clark, R., F. Fanale, and A. Zent (1983), Frost grain size metamorphism: Implications for remote sensing of planetary surfaces, *Icarus*, *56*, 233–245.

Crowe, C., M. Sommerfeld, and Y. Tsuji (1997), *Multiphase Flows with Droplets and Particles*, CRC Press, Boca Raton, Fla.

Fortes, A. D. (2007), Metasomatic clathrate xenoliths as a possible source for the south polar plumes of Enceladus, *Icarus*, *191*, 743–748.

Halevy, I., and S. T. Stewart (2008), Is Enceladus' plume tidally controlled?, *Geophys. Res. Lett.*, *35*, L12203, doi:10.1029/2008GL034349.

Hansen, C., et al. (2008), Water vapour jets inside the plume of gas leaving Enceladus, *Nature*, *456*, 477–479.

Hedman, M. M., P. D. Nicholson, M. R. Showalter, R. H. Brown, B. J. Buratti, and R. N. Clark (2009), Spectral observations of the Enceladus plume with Cassini-VIMS, *Astrophys. J.*, *693*, 1749–1762.

Hurford, T. A., P. Helfenstein, G. V. Hoppa, R. Greenberg, and B. G. Bills (2007), Eruptions arising from tidally controlled periodic openings of rifts on Enceladus, *Nature*, *447*, 292–294.

Ingersoll, A., and A. Pankine (2010), Subsurface heat transfer on Enceladus: Conditions under which melting occurs, *Icarus*, *206*, 594–607.

Jaumann, R., et al. (2008), Distribution of icy particles across Enceladus surface as derived from Cassini-VIMS measurements, *Icarus*, *193*, 407–419.

Kaempfer, T. U., and M. Schneebeli (2007), Observation of isothermal metamorphism of new snow and interpretation as a sintering process, *J. Geophys. Res.*, *112*, D24101, doi:10.1029/2007JD009047.

Kempf, S., U. Beckmann, and J. Schmidt (2010), How the Enceladus dust plume feeds Saturn's E ring, *Icarus*, *206*, 446–457.

Kieffer, S. W., X. Lu, C. M. Bethke, J. R. Spencer, S. Marshak, and A. Navrotsky (2006), A clathrate reservoir hypothesis for Enceladus' south polar plume, *Science*, *314*, 1764–1766.

Nimmo, F., J. R. Spencer, R. T. Pappalardo, and M. E. Mullen (2007), Shear heating as the origin of the plumes and heat flux on Enceladus, *Nature*, *447*, 289–291.

Porco, C. C., et al. (2006), Cassini observes the active south pole on Enceladus, *Science*, *311*, 1393–1401.

Razzaghi, A., et al. (2007), *Enceladus Flagship Mission Concept Study*, NASA Goddard Space Flight Cent., Greenbelt, Md.

Schmidt, J., N. Brilliantov, F. Spahn, and S. Kempf (2008), Slow dust in Enceladus' plume from condensation and wall collisions in tiger stripe fractures, *Nature*, *457*, 685–688.

Spahn, F., et al. (2006), Cassini dust measurements at Enceladus and implications for the origin of the E ring, *Science*, *311*, 1416–1418.

Spencer, J. R., et al. (2006), Cassini encounters Enceladus: Background and the discovery of a south polar hot spot, *Science*, *311*, 1401–1405.

Spencer, J. R., A. C. Barr, L. W. Esposito, P. Helfenstein, A. P. Ingersoll, R. Jaumann, C. P. McKay, F. Nimmo, and J. H. Waite (2009), Enceladus: An active cryovolcanic satellite, in *Saturn From Cassini-Huygens*, edited by M. Dougherty, L. Esposito, and S. Krimigis, pp. 683–724, Springer, Dordrecht, Netherlands.

Waite, J., et al. (2006), Cassini ion and neutral mass spectrometer: Enceladus plume composition and structure, *Science*, *311*, 1419–1422.

W. Degruyter and M. Manga, Earth and Planetary Science and Center for Integrative Planetary Science, University of California, 179 McCone Hall, Berkeley, CA 94720-4767, USA. (wim.degruyter@berkeley.edu)